9746 *Biochemistry* **2010,** *49,* 9746–9755
DOI: 10.1021/bi101000m

BIOCHEMISTRY
including biophysical chemistry & molecular biology
Article

A Natively Unfolded $\beta\gamma$-Crystallin Domain from *Hahella chejuensis*[†]

Atul K. Srivastava,[‡] Yogendra Sharma,[§] and Kandala V. R. Chary*[,‡]

[‡]*Department of Chemical Sciences, Tata Institute of Fundamental Research, Mumbai 400005, India, and* [§]*Center for Cellular and Molecular Biology, Hyderabad 500007, India*

Received June 21, 2010; Revised Manuscript Received October 7, 2010

ABSTRACT: To date, very few $\beta\gamma$-crystallins have been identified and structurally characterized. Several of them have been shown to bind Ca^{2+} and thereby enhance their stability without any significant change in structure. Although Ca^{2+}-induced conformational changes have been reported in two putative $\beta\gamma$-crystallins from *Caulobacter crescentus* and *Yersinia pestis*, they are shown to be partially unstructured, and whether they acquire a $\beta\gamma$-crystallin fold is not known. We describe here a $\beta\gamma$-crystallin domain, hahellin, its Ca^{2+} binding properties and NMR structure. Unlike any other $\beta\gamma$-crystallin, hahellin is characterized as a pre-molten globule (PMG) type of natively unfolded protein domain. It undergoes drastic conformational change and acquires a typical $\beta\gamma$-crystallin fold upon Ca^{2+} binding and hence acts as a Ca^{2+}-regulated conformational switch. However, it does not bind Mg^{2+}. The intrinsically disordered Ca^{2+}-free state and the close structural similarity of Ca^{2+}-bound hahellin to a microbial $\beta\gamma$-crystallin homologue, Protein S, which shows Ca^{2+}-dependent stress response, make it a potential candidate for the cellular functions. This study indicates the presence of a new class of natively unfolded $\beta\gamma$-crystallins and therefore the commencement of the possible functional roles of such proteins in this superfamily.

$\beta\gamma$-Crystallins belong to a superfamily of diverse proteins with members from archaea to vertebrates. These proteins have a topology similar to that of the lens β- and γ-crystallins (*1*). They are thought to have originated from a single-domain ancestor by gene duplication of a characteristic but diverse crystallin type Greek key motif (*2*). Structurally, each domain consists of an eight-strand β-sandwich made of two Greek key motifs (*3*, *4*). The Greek key motif is characterized by a β-hairpin that forms a loop between the first two strands and consists of a partially conserved "Y/FXXXXY/FXG" signature sequence that interacts with a generally conserved serine at the start of the fourth β-strand and provides stability to the scaffold.

The $\beta\gamma$-crystallin superfamily is growing with the addition of new members, but only for a few are the three-dimensional structures available (*5*−*7*). Their physiological functions are not understood, and many have been annotated as hypothetical proteins in their genome. Lens homologues of $\beta\gamma$-crystallins are thought to be largely structural, long-lived proteins with inherent high domain stability (*8*, *9*). One of the features of some of these proteins is the property of Ca^{2+} binding that categorizes these proteins into a separate class of Ca^{2+}-binding proteins (*5*, *10*, *11*). It is largely seen that Ca^{2+} binding provides further stability, as in case of Protein S and Spherulin 3a (*12*, *13*). Therefore, it is possible to extrapolate the function of Ca^{2+} in providing additional stability to the domain. Interestingly, these stable proteins do not generally undergo significant conformational changes upon binding Ca^{2+} (*5*, *14*) unlike other Ca^{2+}-binding sensors, for instance, EF-hand proteins (*15*, *16*). Because the functions of these proteins are not yet known, the structure and their relation with Ca^{2+} binding properties and stability of domains have been an unexplored area of great interest to be investigated further. Thus, it is important to study in detail many more diverse members of this superfamily and understand their individual Ca^{2+} binding characteristics. In this field, the genomes of various organisms, sequenced so far, provide a wealth of information for identifying new members belonging to the $\beta\gamma$-crystallin superfamily.

Against this backdrop, we set out to analyze the genome of a marine bacterium, *Hahella chejuensis*. It secretes a red pigment that has a lytic activity against red-tide dinoflagellate, a serious problem for marine ecosystems and humans (*17*). We observed a protein (GenBank accession number YP_434263) in the genome of *H. chejuensis*, and on the basis of the signature sequence of $\beta\gamma$-crystallin, we identified a domain of 91 amino acid residues (residues 162−252) for cloning and overexpression to avoid the ambiguities that might arise because of other non-crystallin domains of the full-length protein. It has been named hahellin (hahella + crystallin) (*18*).

In this paper, we describe how hahellin is natively unfolded and folds upon binding Ca^{2+} into a well-defined structured form (Ca^{2+}-bound). Because there have been no structural studies for members (*19*, *20*) with such unusual behaviors in the $\beta\gamma$-crystallin superfamily, we set out to investigate the structural details. The extensive characterization of hahellin led it to be defined as a first pre-molten globule (PMG)[1] type intrinsically disordered protein

[†]The facilities provided by the National Facility for High Field NMR, supported by the Department of Science and Technology (DST), the Department of Biotechnology (DBT), the Council of Scientific and Industrial Research (CSIR), and the Tata Institute of Fundamental Research, are gratefully acknowledged.

*To whom correspondence should be addressed: 1-Homi Bhabha Rd., Navy Nagar, Colaba, Mumbai 400005, India. Phone: 91-022-2278 2489. Fax: 91-22-2280 4610. E-mail: chary@tifr.res.in.

[1]Abbreviations: PMG, pre-molten globule; BLAST, Basic Local Alignment Search Tool; EGTA, ethylene glycol tetraacetic acid; CD, circular dichroism; ITC, isothermal titration calorimetry; DSC, differential scanning calorimetry; NMR, nuclear magnetic resonance; PDB, Protein Data Bank; BMRB, Biological Magnetic Resonance Data Bank; NOE, nuclear Overhauser effect; HSQC, heteronuclear single-quantum correlation.

 Published on Web 10/07/2010

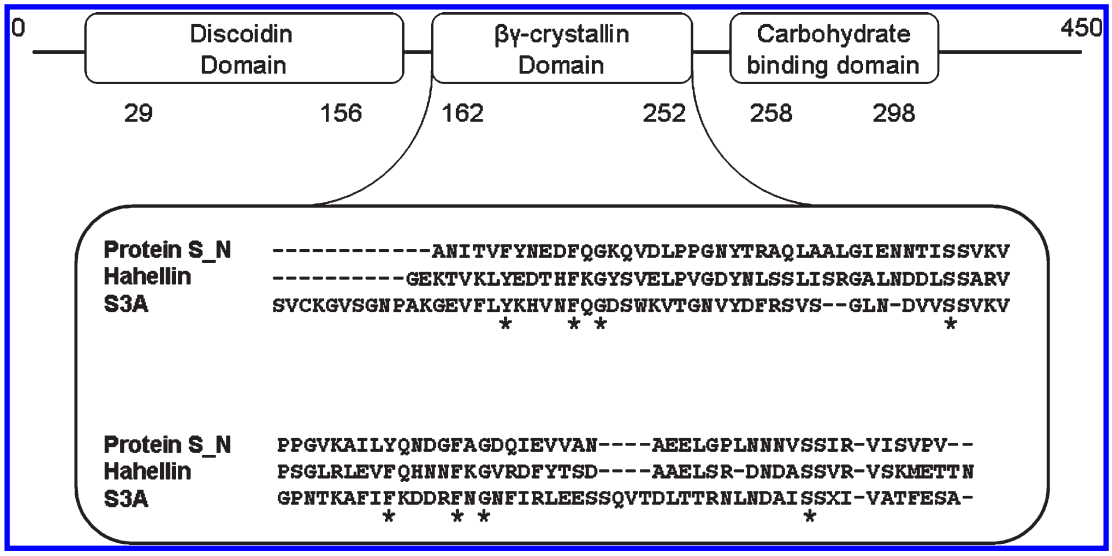

FIGURE 1: Domain organization along the sequence of hahellin (GenBank accession number YP_434263). The three domains are shown by the rounded boxes with their start and end residue numbers. Below is shown the alignment of the $\beta\gamma$-crystallin domain with the sequences of the N-terminal domains of Protein S and Spherulin 3a. The conserved residues in $\beta\gamma$-crystallin type Greek key motifs are denoted with asterisks.

from the $\beta\gamma$-crystallin superfamily. For this very reason, it was not possible to crystallize the protein. Hence, the three-dimensional (3D) NMR structure was determined in its holo form. Ca^{2+} binding induced a compaction with stable secondary and tertiary structures and transformed the unfolded polypeptide chain into a typical $\beta\gamma$-crystallin fold that is similar to other microbial members, such as Protein S and Spherulin 3a, which are known to be involved in the stress response of the respective organisms. The Ca^{2+}-induced conformational transition between natively unfolded apo-hahellin and the stable structure of holo-hahellin is likely to act as a Ca^{2+}-regulated conformational switch and hence to be a key property for the biological functions of hahellin. Further, the existence of hahellin as an intrinsically unstructured protein indicates the possibility of the presence of more such members and hence a new class of intrinsically disordered proteins within the $\beta\gamma$-crystallin superfamily.

MATERIALS AND METHODS

Identification and Selection of the βγ-Crystallin Domain from H. chejuensis. Using the protein sequences of γ-crystallin and other very well established members of the $\beta\gamma$-crystallin superfamily as a template, we performed a BLAST (Basic Local Alignment Search Tool) search against the genome of *H. chejuensis* (strain KCTC 2396) as described previously (*18*). The $\beta\gamma$-crystallin domain is a part of a larger protein of 450 residues as described in Figure 1.

Cloning, Overexpression, Purification, and Isotopic Labeling of Hahellin. The $\beta\gamma$-crystallin domain of hahellin was cloned, overexpressed, and purified as described previously (*18*). Uniformly ^{15}N-labeled, ^{13}C-labeled, and doubly ^{13}C- and ^{15}N-labeled protein samples were produced in M9 minimal medium using $^{15}NH_4Cl$ and D-[$^{13}C_6$]glucose separately and in combination as the sole sources of nitrogen and carbon, respectively. The purification method used was the same as that for the unlabeled protein and has been described previously (*18*). The apo-hahellin was prepared when the protein sample was treated with 1 mM EGTA dissolved in a solution containing 10 mM Tris-HCl and 300 mM NaCl (pH 6.7). EGTA was removed by exchanging the apo-hahellin with the solution without EGTA mentioned above. The buffers were treated with Chelex-100, and plasticware was used to prevent any possible Ca^{2+} contamination. The urea-denatured state was prepared by exchanging the protein solution with a solution containing 8 M urea, 10 mM Tris-HCl, 300 mM NaCl, and 20 mM $CaCl_2$ (pH 6.7) in an ultrafiltration cell using a 1 kDa cutoff membrane at 4 °C.

Circular Dichroism Spectroscopy. CD spectra were recorded on a JASCO J-810 spectropolarimeter (Jasco Ltd., Tokyo, Japan) equipped with a Peltier-controlled temperature controller. The cuvettes with path lengths of 0.1 and 1 cm were used for recording far- and near-UV CD spectra, respectively.

The temperature dependence of both secondary and tertiary structures of the holo form was studied by scanning the ranges of 200−250 and 250−300 nm, respectively. The temperature of the sample was increased from 25 to 80 °C and then decreased from 80 to 25 °C at a rate of 1 °C/min using a programmable Peltier device attached to the thermostated cell holder. The protein concentrations used for far-UV CD and near-UV CD were 20 and 110 μM, respectively. The temperature dependence of the secondary structure of Ca^{2+}-free hahellin was monitored by recording far-UV CD spectra from 195 to 240 nm at temperatures ranging from 10 to 80 °C in steps of 5 °C with a protein concentration of 20 μM.

Ca^{2+} titration experiments were conducted with protein concentrations of 13.5 and 160 μM for far-UV and near-UV spectroscopy, respectively, at 25 °C. All the experiments were performed with freshly prepared samples in 10 mM Tris-HCl buffer (pH 6.75) in the presence or absence of a suitable concentration of Ca^{2+} and NaCl. The CD spectra of respective buffers were subtracted from that of the protein for baseline correction. The proportions of secondary structure elements were calculated using the Reed and Yang models available in a software package supplied with the spectropolarimeter.

Isothermal Titration Calorimetry (*ITC*). Binding of Ca^{2+} to hahellin was investigated using ITC. Dissociation constants were determined from the binding isotherm of the protein in a VP-ITC calorimeter (MicroCal Inc.). Ligand and protein solutions were prepared in 10 mM Tris-HCl and 300 mM NaCl (pH 6.75). Samples were centrifuged and degassed prior to the experiment and examined for precipitation, if any, after the titration. All the titrations were conducted at 25 °C. Apo-hahellin (1.42 mL,

179 μM) in the sample cell was titrated with 25 injections of 10 μL each of 10 mM $CaCl_2$. The interval between two injections was 300 s to ensure the return of the signal to the baseline prior to the next injection. Appropriate buffer titrations (without protein) were conducted to determine the heat of dilution, and the corresponding isotherm was subtracted from the Ca^{2+} binding isotherm. The resulting calorimetric isotherm was deconvoluted for the best-fit model using Origin supplied by MicroCal Inc. For Mg^{2+} binding experiments, a 10 mM $MgCl_2$ solution was injected into a 120 μM protein solution using the same procedure mentioned above.

Size Exclusion Chromatography. Hydrodynamic radii of hahellin were determined under different conditions using a pre-equilibrated Superdex-75 10/30 Tricorn column (GE Healthcare) coupled with a FPLC unit (AKTA FPLC). The equipment included a UV photometer operating at 280 nm for concentration measurement. The column was calibrated using standard molecular mass markers (Sigma). Holo-hahellin was run with a buffer containing 50 mM Tris buffer, 300 mM NaCl, and 20 mM $CaCl_2$ (pH 6.75). The denatured hahellin was run with 8 M urea dissolved in the buffer mentioned above. For the apo-hahellin sample, the $CaCl_2$ was replaced with 1 mM EDTA. All the experiments were performed at 25 °C with a flow rate 0.5 mL/min.

A calibration curve for the molecular mass and elution volume was obtained, and on that basis, the apparent molecular masses of hahellin in different conformational states were determined (eq 1). Similarly, the hydrodynamic radii were obtained with a calibration curve for the molecular mass and the Stokes radii (eq 2).

$$\log(M_r) = 6.50 - 1.36 \log(V_e/V_0) \quad (1)$$

$$\log(R_s) = -0.99 + 0.53 \log(M_r) \quad (2)$$

The theoretical Stokes radii of coil type (R_s^{coil}), pre-molten globule (R_s^{PMG}), and fully unfolded (R_s^{urea}) proteins were determined using eqs 3−5, as described previously (*21*).

$$\log(R_s^{coil}) = -(0.551 \pm 0.032) + (0.493 \pm 0.008) \log(M_r) \quad (3)$$

$$\log(R_s^{PMG}) = -(0.239 \pm 0.055) + (0.403 \pm 0.012) \log(M_r) \quad (4)$$

$$\log(R_s^{urea}) = -(0.649 \pm 0.016) + (0.521 \pm 0.004) \log(M_r) \quad (5)$$

NMR Sample Preparation and NMR Spectroscopy. The details of sample preparation and NMR spectroscopy have been described previously (*24*).

A high-resolution HSQC spectrum of apo-hahellin, with 4096 and 128 complex points in ^1H and ^{15}N dimensions, respectively, was recorded for the determination of the $^3J_{HN-HA}$ coupling constant (*22*). An interleaved two-dimensional $^1H-^{15}N$ NOE experiment with a 4 s recycle delay was performed for the estimation of flexibility in the apo and holo states. The coupling constants and NOE values are plotted against ^{15}N chemical shifts as the sequence specific resonance assignment of the apo-hahellin is not available.

NMR Spectral Assignment and Structure Calculation. The resonance assignments of the backbone and side chain atoms have been described previously (*23*). The $^3J_{HN-HA}$ coupling constants and the corresponding φ torsion angles were obtained using a 3D HNHA spectrum. The torsion angle constraints (φ and ψ) were determined using TALOS, based on the chemical shift information available for $^1H^{\alpha}$, $^{13}C'$, $^{13}C^{\alpha}$, $^{13}C^{\beta}$, and ^{15}N nuclei (*24*). The NOE distance restraints were generated using ^{13}C- and ^{15}N-edited NOESY spectra.

Structure calculations were performed on the basis of 956 non-hydrogen bond and 40 hydrogen bond restraints and 100 dihedral angle restraints (φ and ψ). The upper bounds for all the NOE restraints were set as 5.0 Å. However, no lower bounds were used for these restraints. These distance constraints have the following distribution: 331 intraresidue, 269 sequential, 83 medium-range, and 273 long-range constraints. Hydrogen bond constraints were incorporated only for residues that are involved in a β-sheet, as characterized by chemical shift indices (CSI) and $^3J_{HN-HA}$ values. Upper bounds for H−O and N−O distances were set as 2 and 3 Å, respectively. Structure calculations were performed with a simulated annealing protocol by molecular dynamics simulation in torsion angle space implemented in CYANA (*25*). The final ensemble of structures that represented the 20 best CYANA conformers (based on the lowest target function) obtained from an input of 200 initial structures and 50000 torsion angle dynamics steps was analyzed, and figures were generated with PyMOL (http://www.pymol.org).

Although the structure of Ca^{2+}-bound hahellin was determined, we could not identify the exact coordinating atoms involved in Ca^{2+} binding. Therefore, no Ca^{2+} ligand restraints were used in the structure calculation. However, the residues belonging to the Ca^{2+}-binding sites were identified using Mn^{2+} and Gd^{3+} titrations (Figure 4A,B of the Supporting Information).

Structural Analysis. The stereochemical quality was checked and validated using PSVS program (Protein Structure Validation Software Suite) (http://psvs-1_4-dev.nesg.org/) for the 20 best structures. Atomic coordinates of all 20 structures have been deposited in the Protein Data Bank as entry 2KP5.

RESULTS

Sequence Analysis and Identification of the $\beta\gamma$-Crystallin Domain. The full-length protein is a 450-amino acid hypothetical protein that harbors a putative pair of Greek key motifs forming a $\beta\gamma$-crystallin domain (residues 162−252) (Figure 1) named hahellin. In addition to hahellin, it also contains a discoidin domain (residues 29−155) and a chitin/cellulose binding domain (residues 258−298).

Probing Ca^{2+} Binding by ITC. The quantification of the Ca^{2+} binding stoichiometry and the binding enthalpy of hahellin was conducted by ITC. The associated thermodynamic parameters for the binding reaction, as obtained under our experimental conditions, are listed in Table 1. The Ca^{2+} binding to the protein is an exothermic reaction and follows a sequential two-site model with dissociation constants of ~7 μM (for the high-affinity site) and 120 μM (for the low-affinity site) (Figure 2).

Ca^{2+}-Induced Conformational Changes of Hahellin. The far-UV CD spectrum of hahellin in its apo (Ca^{2+}-free) state was typical of a predominantly unfolded polypeptide chain, as revealed by the strong negative $\pi-\pi^*$ band at ~200 nm (Figure 3A). A very weak negative band in the vicinity of 222 nm due to the $n'-\pi^*$ transition is indicative of the presence of some residual secondary structure elements. Upon addition of Ca^{2+} to apo-hahellin, the secondary structures were formed as revealed by the concomitant decrease in the intensity of the $\pi-\pi^*$ band and the increase in the intensity of the $n'-\pi^*$ band for Ca^{2+}-bound hahellin (holo state) (Figure 3A). The estimated proportions of various secondary structure elements present in apo- and holo-hahellin, as obtained by model fitting (based on

Table 1: Thermodynamic Parameters for Ca^{2+} Binding to Hahellin As Derived from Isothermal Titration Calorimetry

sequential binding site model	K_a (M^{-1})	ΔH (kcal/mol)	ΔS (cal mol^{-1} deg^{-1})
site 1	$(1.45 \pm 0.36) \times 10^5$	-10.17 ± 0.13	-10.5
site 2	$(8.31 \pm 0.29) \times 10^3$	-20.00 ± 0.22	-49.2

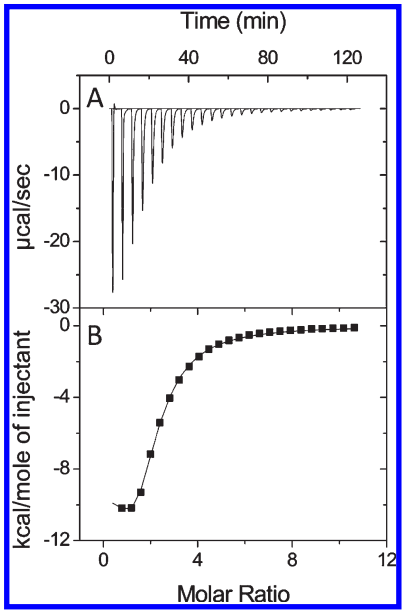

FIGURE 2: Isothermal titration calorimetry of Ca^{2+} binding to hahellin. (A) Calorimetric titration profile of 10 μL aliquots of 10 mM $CaCl_2$ in 179 μM apoprotein in 10 mM Tris-HCl and 300 mM NaCl (pH 6.75) at 25 °C. (B) Least-squares fit of the data to the heat absorbed per mole of titrant vs the ratio of the total concentration of Ca^{2+} to the total concentration of protein. The data were fitted with sequential binding site model. The best fit values of dissociation constants and enthalpies are listed in Table 1.

the method of Yang and Reed), are listed in Table 2. The near-UV CD spectrum of apo-hahellin was featureless and hence indicated the absence of any tertiary structure. However, upon addition of Ca^{2+} to apo-hahellin, very drastic changes in the spectrum were observed because of the defined transitions for Tyr and vibronic peaks for Phe (there is no Trp in this domain) in the holo-hahellin (Figure 3B).

NMR spectroscopy was used to further characterize the Ca^{2+}-induced conformational changes of hahellin. The $^1H-^{15}N$ HSQC spectrum of 8 M urea-denatured hahellin displayed a narrow chemical shift dispersion of $^1H^N$ proton (~0.6 ppm) and ^{15}N resonances (~19 ppm) (Figure 4), with all the peaks appearing at the expected frequencies for an unfolded polypeptide, the so-called random coil chemical shifts. The low chemical shift dispersion was consistent with a protein with no stable secondary or tertiary structures. The spectrum of apo-hahellin under native conditions also exhibited very narrow $^1H^N$ chemical shift dispersion (Figure 4) and resembled that of the hahellin denatured in 8 M urea, with narrow line widths. The amide vectors (N−H moieties) of the protein exhibited high flexibility as indicated by the low $^1H-^{15}N$ NOE values (0.5 to −1.0) (Figure 5A). The heteronuclear NOE gives direct evidence that apo-hahellin has a higher degree of dynamic flexibility with respect to the overall tumbling of the protein. The $^3J_{HN-HA}$ coupling constants determined for further assessment of the conformational space accessed by apo-hahellin lie in the range of 5−8 Hz (Figure 5B), which is expected for a protein with random coil conformations (*26*).

The $^{15}N-^1H$ HSQC spectrum of holo-hahellin was entirely different. The chemical shift dispersion of $^1H^N$ increased to ~4 ppm and that of ^{15}N to ~26 ppm with simultaneous increases in the line widths, which are all typical of a well-folded protein (Figure 4). The motional rigidity of the protein is expressed by the high (~0.8) values of the $^1H-^{15}N$ NOE (Figure 6). A few residues at the end of the C-terminus, however, show very low NOE values (from 0.5 to −0.4), indicating a highly flexible stretch at the end of the C-terminus.

The NMR and CD data demonstrate that apo-hahellin is predominantly unfolded with some residual secondary structure and an almost complete absence of tertiary structure, while Ca^{2+} binding induced the folding of the protein into a compact and rigid β-sheet-rich (~70%) conformation.

Ca^{2+}-Induced Hydrodynamic Changes of Hahellin. The hydrodynamic radii for holo-hahellin, apo-hahellin, and urea-denatured hahellin were determined using size exclusion chromatography (SEC). As shown in Figure 7, holo-hahellin eluted at a retention volume of 14 mL, which is close to that expected for a globular protein of 10 kDa. In contrast, apo-hahellin eluted at a retention volume of 12.5 mL, a value that corresponds to a globular protein of 20 kDa. The retention volume was 10.38 mL in the case of hahellin denatured with 8 M urea.

The hydrodynamic radii determined by the calibration curve for the SEC column were 15, 20.41, and 28.67 Å for holo-hahellin, apo-hahellin, and urea-denatured hahellin, respectively. These experimentally derived radii were compared with those of theoretically obtained values (using eqs 3−5) for pre-molten globule (23.79 Å), coil type (26.62 Å), and fully unfolded (urea-denatured) (27.5 Å) conformations of a protein with a molecular mass of 10.2 kDa (M_r of hahellin).

Ca^{2+}-Induced Stability and Thermal Folding of Apo-Hahellin. Thermally induced unfolding of hahellin was monitored by far-UV and near-UV CD. The ellipticity values at 232 and 275 nm were used to follow the unfolding of hahellin. The temperature of half-melting (T_m) was then determined to be 50 °C (Figure 3 of the Supporting Information).

For holo-hahellin (saturated with 20 mM Ca^{2+}), the thermal unfolding with a concomitant decrease in the level of secondary and tertiary structure was typical of a globular protein domain. However, in marked contrast, our attempts to unfold apo-hahellin resulted in a decrease in the intensity of the negative band at 200 nm and an increase in the intensity of the negative band at 222 nm. This showed the formation of secondary structures in apo-hahellin when heated (Figure 8).

Double-Wavelength Plot for ApoHahellin. The double-wavelength plot was generated by plotting the molar ellipticity per residue at 222 nm against that at 200 nm for many intrinsically unstructured proteins along with that of apo-hahellin; the corresponding ellipticity values for apo-hahellin were 1865 and 13186 deg cm^2 $dmol^{-1}$, respectively (Figure 9). The data used in the double-wavelength plot for other proteins were taken from the literature (*27*).

Structure of the $\beta\gamma$-Crystalllin Domain of Hahellin. The 3D solution structure of holo-hahellin was determined by

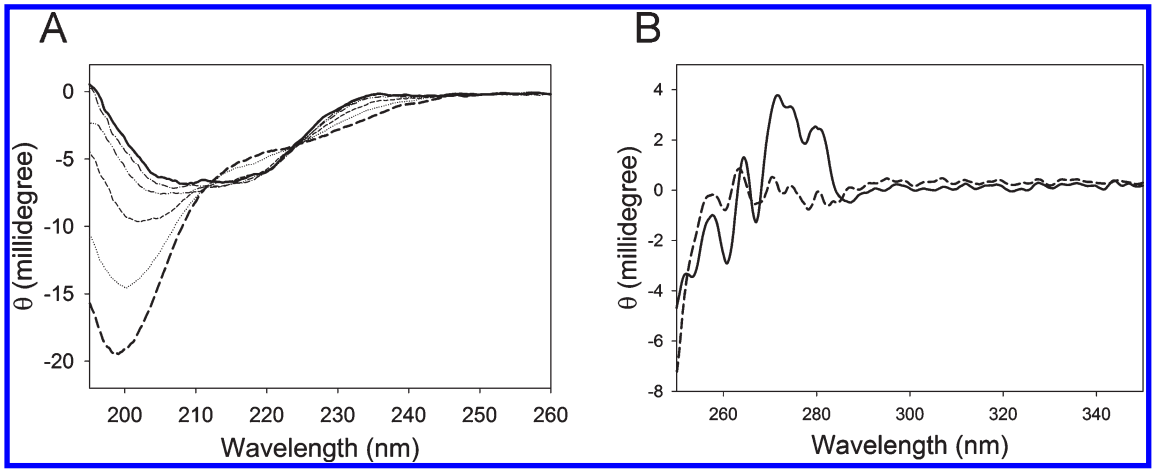

FIGURE 3: Effect of Ca^{2+} binding on far- and near-UV CD spectra of hahellin. (A) Changes in the far-UV CD spectra of apo-hahellin upon addition of Ca^{2+} at the following concentrations: 0 (thick dashed line), 100, 200, 300, 400, and 500 μM (thick solid line). The protein concentration was 13.5 μM, and the cell path length was 0.1 cm. (B) Near-UV CD spectra recorded for Ca^{2+}-free (– – –) and Ca^{2+}-bound (—) hahellin. The protein concentration was 160 μM, and the cell path length was 1 cm.

Table 2: Estimates (percent) of Secondary Structure Elements Calculated from Far-UV CD Spectra

model for curve fitting	helix	β-strand	random coil	turn
Reed[a]	8.1	15.2	76.7	0.0
Yang[a]	0.0	18.0	64.0	18.0
Reed[b]	4.0	34.9	42.3	18.9
Yang[b]	7.9	69.3	17.4	5.4

[a]Ca^{2+}-free hahellin. [b]Ca^{2+}-bound hahellin.

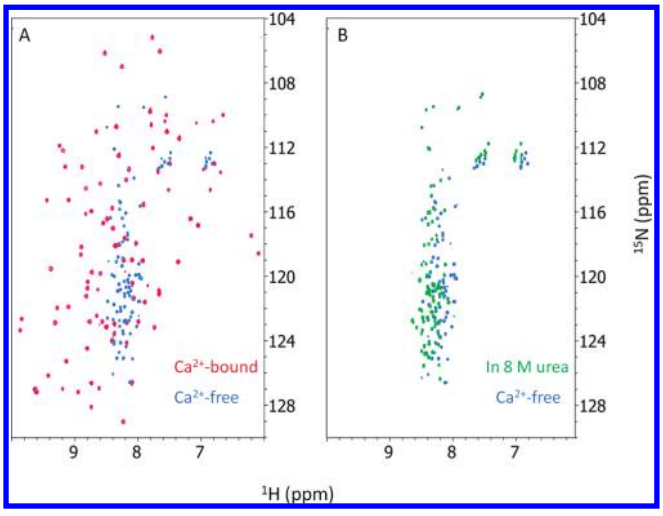

FIGURE 4: Different conformational states of hahellin characterized by NMR. Two-dimensional HSQC spectrum of apo-hahellin overlaid with the HSQC spectra of (A) the Ca^{2+}-bound state (red) and (B) the 8 M urea-denatured state (green) for comparison, in 10 mM Tris-HCl and 300 mM NaCl (pH 6.75). The spread of peaks along the proton dimension is ~0.6 ppm in the spectra of Ca^{2+}-free and urea-denatured hahellin, while in the Ca^{2+}-bound form, the dispersion is large (~4.2 ppm).

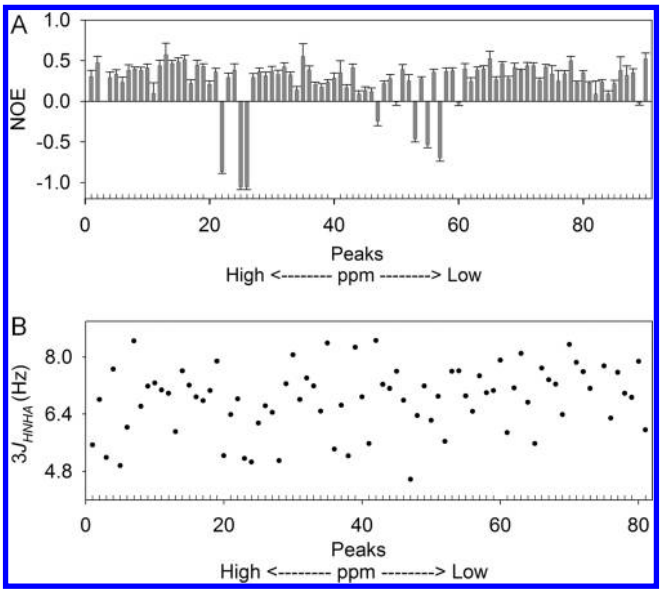

FIGURE 5: (A) Heteronuclear $\{^1H\}-^{15}N$ NOE data for apo-hahellin. The histograms are sorted by ^{15}N chemical shifts. (B) $^3J_{HN-HA}$ coupling constants for apo-hahellin plotted for peaks that are sorted by ^{15}N chemical shifts.

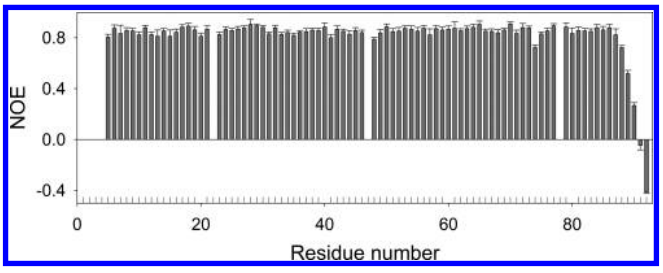

FIGURE 6: Heteronuclear $\{^1H\}-^{15}N$ NOE data for holo-hahellin. The bars are sorted by residue number.

multidimensional heteronuclear NMR spectroscopy. ^1H, ^{13}C, and ^{15}N resonance assignments (>95%) were obtained for all but the first three residues using a suite of double- and triple-resonance backbone-based scalar correlated experiments as described previously (*23*). Qualitative analysis of the pattern of the NOE revealed the presence of an α-helix and seven β-strands (data not shown), which was fully consistent with the analysis by chemical shift index.

The structure was calculated on the basis of NOEs and dihedral angles derived form chemical shifts using CYANA as described in Materials and Methods. The final ensemble of 20

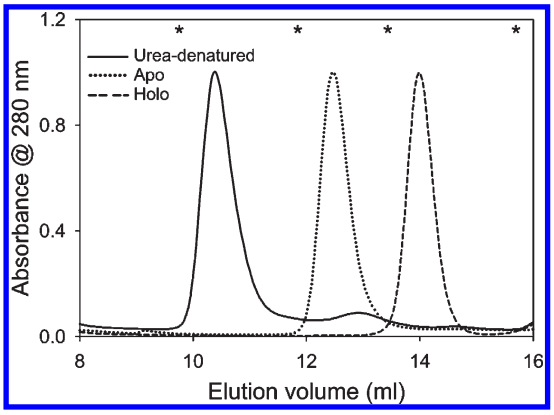

FIGURE 7: Hydrodynamic characterization of hahellin. Size exclusion chromatography elution profile of hahellin monitored at 280 nm. Asterisks denote the positions of the molecular mass standards: bovine serum albumin (66.0 kDa), carbonic anhydrase (29.0 kDa), cytochrome *c* (12.4 kDa), and aprotinin (6.5 kDa) from left to right, respectively.

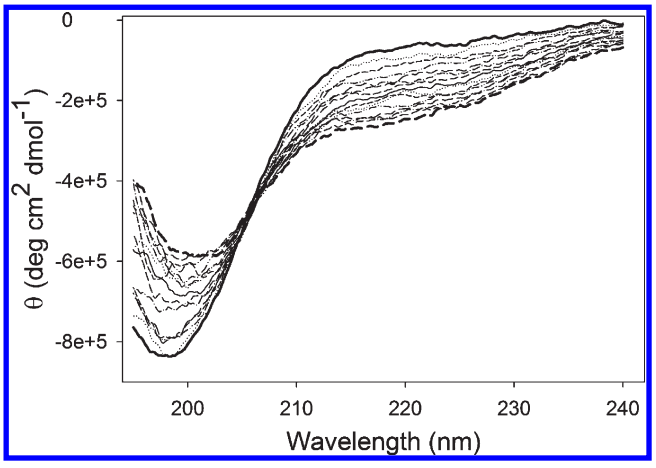

FIGURE 8: Thermally induced secondary structure formation in apo-hahellin. Far-UV CD spectra of Ca^{2+}-free hahellin recorded at different increasing temperatures ranging from 10 to 80 °C with steps of 5 °C in 10 mM Tris-HCl (pH 6.75). The protein concentration used was 20 μM, and the cell path length was 0.1 cm. The spectra at 10 °C (thick solid line) and 80 °C (thick dashed line) are shown to illustrate the net change in secondary structure with an increase in temperature.

structures (Figure 10A) was selected on the basis of least restraint violation and minimum total molecular energy. The ensemble is well-defined and exhibits a low constraint violation energy with no distance violations of >0.1 Å, no dihedral angle violations of >3°, and one van der Waals violation of >0.1 Å. The quality of the structures in regions of secondary structure is good, with a root-mean-square deviation (rmsd) of 0.5 Å for regions of secondary structure backbone atoms (Figure 10A). Overall, the backbone rmsd is 1.2 Å. For heavy atoms, the rmsds are 1.0 Å for regions of secondary structure and 1.6 Å for all heavy atoms.

The good quality of the structure is further reflected by PROCHECK (included in PSVS program) analysis; for instance, 79.9% of all the backbone torsion angles are in the most favored region, 18.1% in additionally allowed regions, and only 2% in generously allowed regions of the Ramachandran plot. The structural statistics of all 20 conformers are listed in Table 3.

The structure is composed of a short α-helix (residues 27−33) and seven β-strands (a−f and h), consisting of residues 5−8, 17−20, 23−25, 41−44, 50−54, 64−66, and 81−85, respectively. These β-strands form two antiparallel β-sheets resulting in a

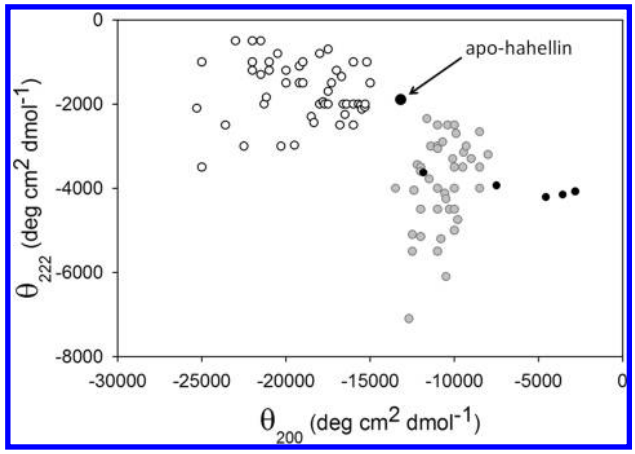

FIGURE 9: Double-wavelength plot created by plotting the molar ellipticity per residue at 200 and 222 nm along the abscissa and ordinate, respectively, for 96 proteins, including hahellin. Empty circles and filled (gray) circles represent the positions of coil type and pre-molten globule type intrinsically unstructured proteins, respectively. The data were taken from ref *27*. Apo-hahellin is marked with an arrow. The black filled circles, from left to right, correspond to hahellin in the presence different concentrations of Ca^{2+} (100, 200, 300, 400, and 500 μM, respectively).

sandwichlike structure with the small α-helix (Figure 10B,C). It is to be noted that the β-strands in the structure are not in a sequential order. The first β-sheet consists of strands a, b, and d strand, and the other consists of strands c, h, e, and f. These secondary structure elements are distributed in the structure with the help of coiled loops and β-hairpins connecting the β-strands.

The topology created by the arrangement of the β-strands in hahellin is illustrated in a schematic (Figure 10B) and is well-identified with the $\beta\gamma$-crystallin fold produced due to intercalation of two Greek key motifs. Here, one β-strand (g) that is present in a standard Greek key otherwise is not developed. The first Greek key motif in hahellin is characterized by a β-hairpin (Y8−G15) that forms a loop between strands a and b and interacts with a conserved Ser residue at position 42 (S42) at the start of β-strand d. The second motif uses another β-hairpin (F54−G61) to form a loop between strands e and f and interacts with S81. There is small local motif, tyrosine corner, that is composed of G23, D24, and Y25 between strands b and c.

DISCUSSION

Many members of the $\beta\gamma$-crystallin superfamily have been shown to bind Ca^{2+} with a range of affinities (*28*), and in a recent study, the crystallin type Greek key motif with the sequence N/D-N/D-X-X-S/T-S has been shown to be a Ca^{2+}-binding motif (*5*, *11*). Via analysis of the amino acid sequence of hahellin, two homologous stretches of sequence, N37-DDL-S42 and D76-NDA-S80, were identified, which in turn led us to perform Ca^{2+} binding studies using various biophysical methods.

There are two Ca^{2+}-binding sites, but the affinity for one site is in the submillimolar range. As the protein is unfolded in the apo form, the interpretation of the apparent Ca^{2+} binding affinities becomes complicated because of the coupled binding and folding processes. However, the large negative entropy and enthalpy changes are due to the formation of structure from an unfolded protein with concomitant binding of Ca^{2+}. Hahellin does not bind Mg^{2+} as demonstrated by CD and ITC experiments (data not shown). This shows the specificity of hahellin toward Ca^{2+},

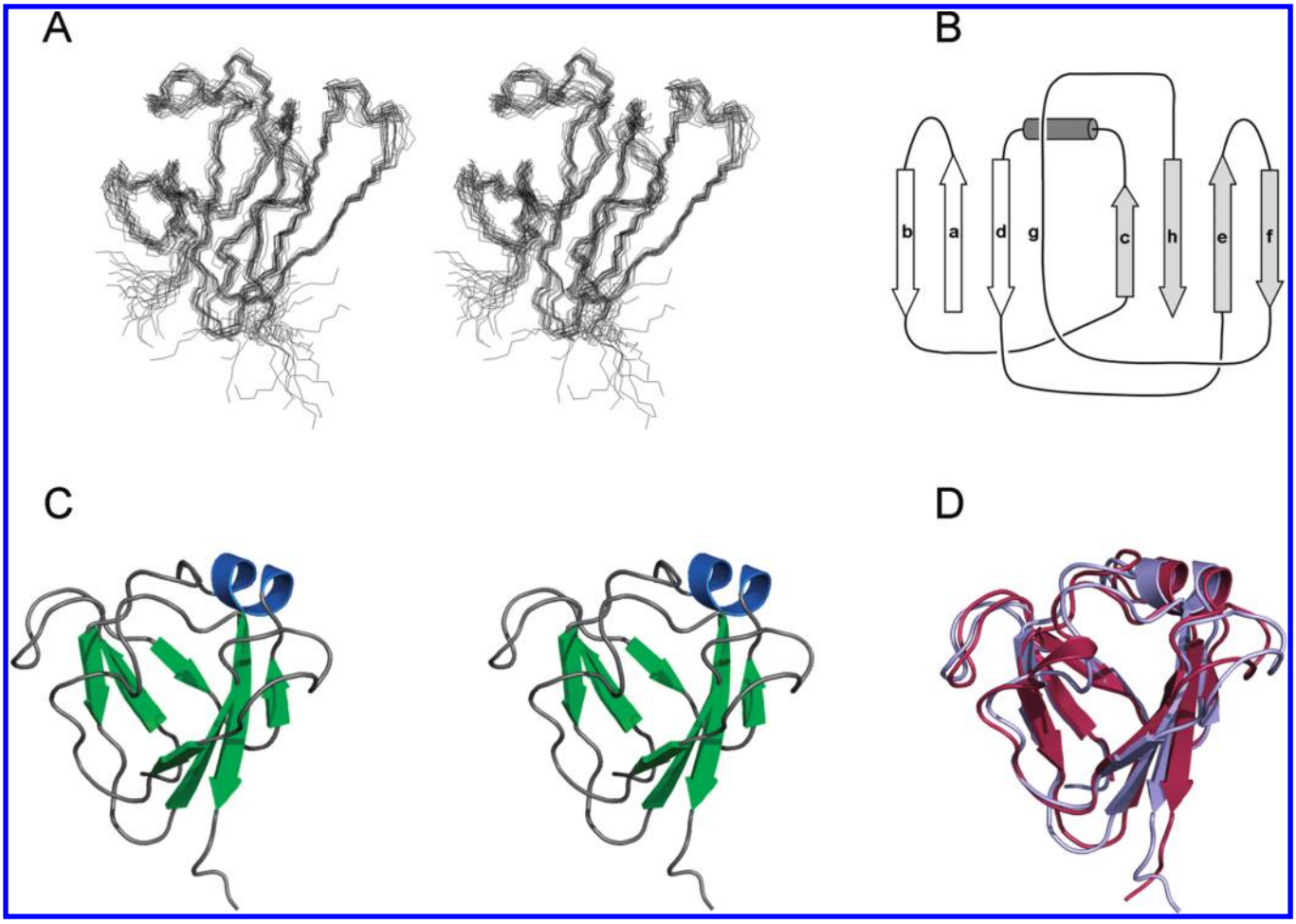

FIGURE 10: (A) Stereo depiction (cross eye) of the 20 best structures of the $\beta\gamma$-crystallin domain of hahellin obtained by simulated annealing. The atomic coordinates have been deposited in the Protein Data Bank as entry 2KP5. (B) Greek key topology. The front β-sheet is composed of β-strands a, b, and d. The rear sheet is composed of strands c, h, e, and f. The small helix is in the top left of the molecule. (C) Stereo depiction (cross eye) of the ribbon diagram of the mean structure of the $\beta\gamma$-crystallin domain of hahellin. The β-strands are colored green; the helix is colored blue, and the loops are colored gray. (D) Structure alignment of the crystallin domain of hahellin with the N-terminal domain of Protein S. The ribbon diagram of the crystallin domain of hahellin (light purple) is aligned with that of Protein S (chocolate) (PDB entry 1NPS) using DALI.

which might be due to the fine-tuning of some residual structure present in the apo form of the protein for initial Ca^{2+} binding.

$\beta\gamma$-Crystallin domains are β-sheet-rich structured proteins in both the Ca^{2+}-free and Ca^{2+}-bound forms, but interestingly, hahellin is devoid of any secondary or tertiary structure in its apo state. However, addition of Ca^{2+} drastically changes hahellin from an unfolded to a folded state with simultaneous formation of secondary and tertiary structures. The conformational transition between the apo and holo states of hahellin is also associated with a change in dynamics. The apo-hahellin is very flexible, which is necessary for being disordered, whereas the holo-hahellin exists as a rigid globular conformation.

Because the far-UV CD resembled that of an unfolded polypeptide chain, it was imperative to search for the signatures of intrinsic disorder in the protein even though such disorder is not expected in the $\beta\gamma$-crystallin superfamily. A very peculiar feature of such intrinsically disordered proteins (IDPs) is the partial folding when they are subjected to extreme conditions of thermal perturbation (*29*). Apo-hahellin acquires secondary structure when heated possibly because of stronger hydrophobic interactions at higher temperatures. It confirms that apo-hahellin is not a usual Ca^{2+}-free protein as found in most of the Ca^{2+}-binding proteins where the apo form is in the molten globule state and shows a distinct transition to a rather completely unfolded conformation. A similar secondary structure formation induced by pH and counterion was observed (see the Supporting Information).

As shown by Uversky et al., the IDPs can be subdivided into separate groups of coil-like and PMG-like proteins based on their hydrodynamic volume and ratio of ellipticity at 200 to that at 222 nm (*30*). The hydrodynamic volumes as determined by size exclusion chromatography (SEC) were ~14130 and ~35595 $Å^3$ for the holo- and apoprotein, respectively. It has been established that the molten globule, on average, is compact and does not increase more than 50% in hydrodynamic volume when compared to its ordered state (*31*). The hydrodynamic radius of hahellin in the fully extended (in 8 M urea, 28.67 Å) conformation is significantly larger than that of the apo state (20.41 Å). It suggests that apo-hahellin possesses some residual structure and belongs to a class of PMG type natively unfolded proteins, which is further confirmed by its position on a double-wavelength plot. The residual structure and the consequent intramolecular interaction of PMG-like apo-hahellin may allow an efficient start of the folding process induced by Ca^{2+} (*32*, *33*). Thus, the functional relevance of the PMG state of apo-hahellin may reside in a more pronounced propensity to undergo induced folding compared to a random coil-like structure.

The observation of Ca^{2+}-induced folding of a natively unfolded protein to a compact globular state has not yet been reported in the $\beta\gamma$-crystallin superfamily, and hence, that demands detailed

Table 3: Structural Statistics for the Ensemble of 20 Refined Conformers of the $\beta\gamma$-Crystallin Domain of Hahellin

no. of constraints used in structure calculation	
NOE constraints	
total interproton restraints	956
intraresidue ($\|i-j\| = 0$)	331
sequential ($\|i-j\| = 1$)	269
medium-range ($1 < \|i-j\| < 5$)	83
long-range ($5 \leq \|i-j\|$)	273
hydrogen bonds	40
torsion angle constraints (φ and ψ)	100
average CYANA target function (Å^2)	0.68 ± 0.20
no. of constraint violations	
NOE distance violations of >0.1 Å	none
van der Waals violations of >0.1 Å	1
dihedral angle violations of $>3°$	none

	rmsd (Å)	
	all residues	ordered residues
all backbone atoms	1.2	0.5
all heavy atoms	1.6	1.0

Ramachandran analysis for non-Gly and non-Pro residues from Procheck[a] (%)	
most favored regions	79.9
additionally allowed regions	18.1
generously allowed regions	2.0
disallowed regions	0.0

Structure Quality Factors (overall statistics)

	mean score for all models	standard deviation	Z score[c]
PROCHECK G factor[b] (ϕ and ψ only)	−0.79	not available	−2.79
PROCHECK G factor[b] (all dihedral angles)	−1.01	not available	−5.97
Verify3D	0.40	0.0244	−0.96
ProsaII (-ve)	0.39	0.0571	−1.08
MolProbity clashscore	21.56	3.4774	−2.17

[a]Ordered residue ranges: 4−10, 16−21, 23−35, 39−56, 62−73, and 79−86. [b]Residues with a sum of ϕ and ψ order parameters of >1.8. [c]With respect to the mean and standard deviation for a set of 252 X-ray structures of <500 residues, with a resolution of ≤ 1.80 Å, an R factor of ≤ 0.25, and an R_{free} of ≤ 0.28; a positive value indicates a "better" score.

conformational studies. As described in Materials and Methods, the hydrodynamic radius of Ca^{2+}-bound hahellin (15 Å) is what is expected for a well-folded globular domain with a molecular mass of ~10 kDa. Further, holo-hahellin is in a stable conformation ($T_m \sim 51$ °C), and the thermal unfolding was found to be cooperative as determined by DSC experiments (data not shown). Therefore, on the basis of all these results, we assign hahellin as a natively unfolded protein that exhibits a disorder−order transition regulated by Ca^{2+}. The physicochemical behavior of hahellin in the full-length protein is not expected to change much as many of the $\beta\gamma$-crystallin domains have been shown to undergo independent folding and are not influenced when studied in the presence of other domains.

The unusual features of hahellin mentioned above, namely, intrinsically unstructured protein and requirement of Ca^{2+} for folding, make it a unique member of the $\beta\gamma$-crystallin superfamily. The structural features of such proteins of the superfamily are not yet available. Therefore, it was of utmost interest to determine its 3D structure. We may add here that our efforts to crystallize hahellin for X-ray crystallography did not succeed, and hence, we chose NMR spectroscopy to determine its structure in solution. Finally, it was remarkable to see the structure of hahellin with almost all the features of a typical $\beta\gamma$-crystallin domain.

The structure of hahellin is stabilized by the intense network of hydrogen bonds between various β-strands as there are no cysteine residues to provide disulfide cross-linking to hold the two β-sheets against each other, which has been shown in several $\beta\gamma$-crystallins (*34*). Its structure is further fortified by Ca^{2+} binding that locks the flexible loops of both the Greek key motifs. As a characteristic feature of such a motif, there is a tyrosine corner in the first Greek key that might be involved in the initial Ca^{2+}-induced folding as suggested previously (*35*). The presence of the tyrosine corner in the first Greek key (N-terminal) makes it B type and, therefore, the arrangement of the Greek keys as BA type, in contrast to lens $\beta\gamma$-crystallins where it is AB type (*36*).

Hahellin is found to be very similar to the N-terminal domain of Protein S as revealed by 3D structural alignment (rmsd of 1.6 Å and Z score of 13.8 for the N-terminal domain, PDB entry 1NPS) (http://ekhidna.biocenter.helsinki.fi/dali_server/). The presence of the small helix is also common in both structures (Figure 10D). Because the $\beta\gamma$-crystallin fold is well-established in Protein S, its striking similarity with hahellin strongly suggests that hahellin is a new bona fide member of the $\beta\gamma$-crystallin superfamily. Because the Greek key motif is involved in Ca^{2+} binding of Protein S (*37*), we have attributed a similar kind of Ca^{2+} binding to hahellin. This is also supported by the data of Ca^{2+} displacement with the paramagnetic Mn^{2+} and Gd^{3+} (Figure 11A,B).

Hahellin is a new addition to the rapidly growing class of natively unfolded proteins with a unique function dependent

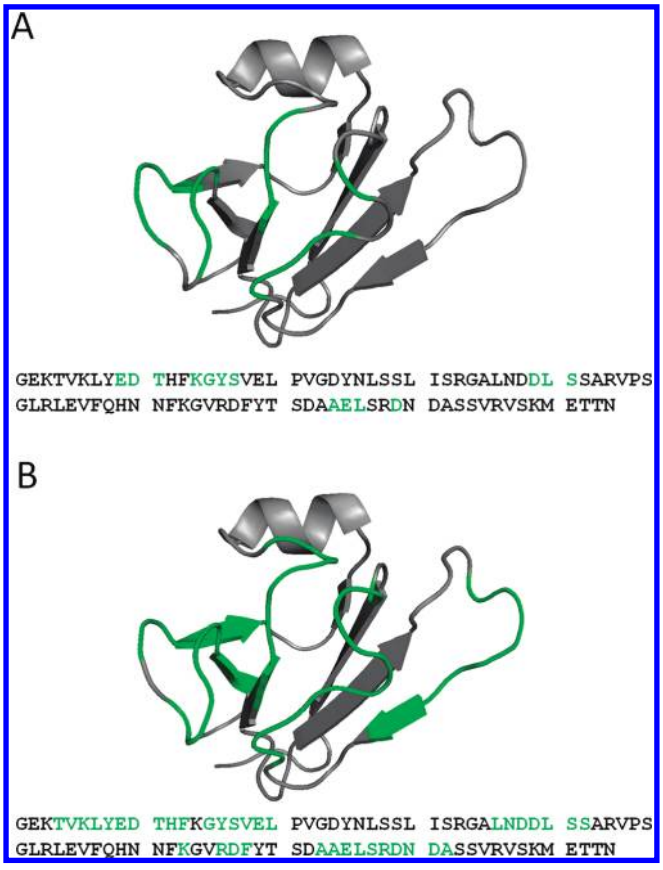

FIGURE 11: Locations of the Ca^{2+}-binding sites in hahellin. The calcium binding residues identified by Mn^{2+} (A) and that obtained by Gd^{3+} (B) are colored green in the ribbon diagram and also highlighted (green) in the sequence. Mn^{2+} could not displace Ca^{2+} from the second site.

on Ca^{2+}. There are very few protein domains that are intrinsically unstructured in the apo form and turn into well-folded compact structures upon Ca^{2+} binding, for instance, calreticulin (*38*, *39*) and osteocalcin (*40*). This indicates the relevance of such a protein for physiological functions.

In conclusion, we describe for the first time a natively unfolded $\beta\gamma$-crystallin domain, an unusual member, because $\beta\gamma$-cytalllins are thought to have evolved as well-structured stable domains. Despite hahellin's unique feature of being natively unfolded, the solution structure in its holo state is very similar to that of microbial homologues such as Protein S. Hahellin shows a disorder−order transition and hence acts as a conformational switch regulated by Ca^{2+}, which might be crucial for its function. The study of such natively unfolded domains is important for our understanding of the sequence−structure relationship for proteins in general as well as for the $\beta\gamma$-crystallin superfamily, in particular, as these unstructured domains cannot be identified on the basis of sequence comparison or other bioinformatic methods.

ACKNOWLEDGMENT

We thank Prof. Jihyun F. Kim (21C Frontier Microbial Genomics and Applications, Center, Korea Research Institute of Bioscience and Biotechnology, Daejeon, Republic of Korea) for providing the genomic DNA of *H. chejuensis*.

SUPPORTING INFORMATION AVAILABLE

Far-UV CD spectrum of hahellin in 8 M urea; effect of pH, NaCl, and KCl on the conformation of Ca^{2+}-free hahellin and thermal denaturation curve of Ca^{2+}-bound hahellin as monitored by far-UV CD; overlay of $^{15}N-^{1}H$ HSQC spectra of Ca^{2+}-bound hahellin recorded with 0 and 2.2 mM $GdCl_3$; overlay of $^{15}N-^{1}H$ HSQC spectra of hahellin recorded with 0 and 2.6 mM $MnCl_2$; and an assigned $^{15}N-^{1}H$ HSQC spectrum of hahellin in the Ca^{2+}-bound form. This material is available free of charge via the Internet at http://pubs.acs.org.

REFERENCES

1. Bloemendal, H., de Jong, W., Jaenicke, R., Lubsen, N. H., Slingsby, C., and Tardieu, A. (2004) Ageing and vision: Structure, stability and function of lens crystallins. *Prog. Biophys. Mol. Biol. 86*, 407–485.
2. Wistow, G. (1990) Evolution of a protein superfamily: Relationships between vertebrate lens crystallins and microorganism dormancy proteins. *J. Mol. Evol. 30*, 140–145.
3. Blundell, T., Lindley, P., Miller, L., Moss, D., Slingsby, C., Tickle, I., Turnell, B., and Wistow, G. (1981) The molecular structure and stability of the eye lens: X-ray analysis of γ-crystallin II. *Nature 289*, 771–777.
4. Wistow, G., Turnell, B., Summers, L., Slingsby, C., Moss, D., Miller, L., Lindley, P., and Blundell, T. (1983) X-ray analysis of the eye lens protein γ-II crystallin at 1.9 Å resolution. *J. Mol. Biol. 170*, 175–202.
5. Aravind, P., Mishra, A., Suman, S. K., Jobby, M. K., Sankaranarayanan, R., and Sharma, Y. (2009) The $\beta\gamma$-crystallin superfamily contains a universal motif for binding calcium. *Biochemistry 48*, 12180–12190.
6. Wenk, M., Baumgartner, R., Holak, T. A., Huber, R., Jaenicke, R., and Mayr, E. M. (1999) The domains of protein S from *Myxococcus xanthus*: Structure, stability and interactions. *J. Mol. Biol. 286*, 1533–1545.
7. Rosinke, B., Renner, C., Mayr, E. M., Jaenicke, R., and Holak, T. A. (1997) Ca^{2+}-loaded spherulin 3a from *Physarum polycephalum* adopts the prototype γ-crystallin fold in aqueous solution. *J. Mol. Biol. 271*, 645–655.
8. Jaenicke, R. (1999) Stability and folding of domain proteins. *Prog. Biophys. Mol. Biol. 71*, 155–241.
9. Jaenicke, R., and Slingsby, C. (2001) Lens crystallins and their microbial homologs: Structure, stability, and function. *Crit. Rev. Biochem. Mol. Biol. 36*, 435–499.
10. Clout, N. J., Kretschmar, M., Jaenicke, R., and Slingsby, C. (2001) Crystal structure of the calcium-loaded spherulin 3a dimer sheds light on the evolution of the eye lens $\beta\gamma$-crystallin domain fold. *Structure 9*, 115–124.
11. Rajini, B., Shridas, P., Sundari, C. S., Muralidhar, D., Chandani, S., Thomas, F., and Sharma, Y. (2001) Calcium binding properties of γ-crystallin: Calcium ion binds at the Greek key $\beta\gamma$-crystallin fold. *J. Biol. Chem. 276*, 38464–38471.
12. Wenk, M., and Mayr, E. M. (1998) *Myxococcus xanthus* spore coat protein S, a stress-induced member of the $\beta\gamma$-crystallin superfamily, gains stability from binding of calcium ions. *Eur. J. Biochem. 255*, 604–610.
13. Kretschmar, M., Mayr, E. M., and Jaenicke, R. (1999) Kinetic and thermodynamic stabilization of the $\beta\gamma$-crystallin homolog spherulin 3a from *Physarum polycephalum* by calcium binding. *J. Mol. Biol. 289*, 701–705.
14. Barnwal, R. P., Jobby, M. K., Devi, K. M., Sharma, Y., and Chary, K. V. (2009) Solution structure and calcium-binding properties of M-crystallin, a primordial $\beta\gamma$-crystallin from archaea. *J. Mol. Biol. 386*, 675–689.
15. Mukherjee, S., Kuchroo, K., and Chary, K. V. (2005) Structural characterization of the apo form of a calcium binding protein from *Entamoeba histolytica* by hydrogen exchange and its folding to the holo state. *Biochemistry 44*, 11636–11645.
16. Chin, D., and Means, A. R. (2000) Calmodulin: A prototypical calcium sensor. *Trends Cell Biol. 10*, 322–328.
17. Jeong, H., Yim, J. H., Lee, C., Choi, S. H., Park, Y. K., Yoon, S. H., Hur, C. G., Kang, H. Y., Kim, D., Lee, H. H., Park, K. H., Park, S. H., Park, H. S., Lee, H. K., Oh, T. K., and Kim, J. F. (2005) Genomic blueprint of *Hahella chejuensis*, a marine microbe producing an algicidal agent. *Nucleic Acids Res. 33*, 7066–7073.
18. Srivastava, A. K., Sharma, Y., and Chary, K. V. (2008) Overexpression, on-column refolding and isotopic labeling of Hahellin from *Hahella chejuensis*, a putative member of the $\beta\gamma$-crystallin superfamily. *Protein Expression Purif. 58*, 269–274.
19. Jobby, M. K., and Sharma, Y. (2005) Calcium-binding crystallins from *Yersinia pestis*. Characterization of two single $\beta\gamma$-crystallin domains of a putative exported protein. *J. Biol. Chem. 280*, 1209–1216.

20. Jobby, M. K., and Sharma, Y. (2007) Caulollins from *Caulobacter crescentus*, a pair of partially unstructured proteins of $\beta\gamma$-crystallin superfamily, gain structure upon binding calcium. *Biochemistry 46*, 12298–12307.
21. Uversky, V. N. (2002) What does it mean to be natively unfolded? *Eur. J. Biochem. 269*, 2–12.
22. Arcus, V. L., Vuilleumier, S., Freund, S. M., Bycroft, M., and Fersht, A. R. (1994) Toward solving the folding pathway of barnase: The complete backbone ^{13}C, ^{15}N, and ^{1}H NMR assignments of its pH-denatured state. *Proc. Natl. Acad. Sci. U.S.A. 91*, 9412–9416.
23. Srivastava, A. K., Sharma, Y., and Chary, K. V. (2008) Sequence specific ^{1}H, ^{13}C, and ^{15}N resonance assignments of Hahellin from *Hahella chejuensis*, a putative member of the $\beta\gamma$-crystallin superfamily. *Biomol. NMR Assignments 2*, 151–153.
24. Cornilescu, G., Delaglio, F., and Bax, A. (1999) Protein backbone angle restraints from searching a database for chemical shift and sequence homology. *J. Biomol. NMR 13*, 289–302.
25. Guntert, P. (2004) Automated NMR structure calculation with CYANA. *Methods Mol. Biol. 278*, 353–378.
26. Smith, L. J., Bolin, K. A., Schwalbe, H., MacArthur, M. W., Thornton, J. M., and Dobson, C. M. (1996) Analysis of main chain torsion angles in proteins: Prediction of NMR coupling constants for native and random coil conformations. *J. Mol. Biol. 255*, 494 506.
27. Uversky, V. N. (2002) Natively unfolded proteins: A point where biology waits for physics. *Protein Sci. 11*, 739–756.
28. Jobby, M. K., and Sharma, Y. (2007) Calcium-binding to lens βB2- and βA3-crystallins suggests that all β-crystallins are calcium-binding proteins. *FEBS J. 274*, 4135–4147.
29. Uversky, V. N., Li, J., and Fink, A. L. (2001) Evidence for a partially folded intermediate in α-synuclein fibril formation. *J. Biol. Chem. 276*, 10737–10744.
30. Uversky, V. N. (2003) Protein folding revisited. A polypeptide chain at the folding-misfolding-nonfolding cross-roads: Which way to go? *Cell. Mol. Life Sci. 60*, 1852–1871.
31. Ptitsyn, O. B. (1995) Molten globule and protein folding. *Adv. Protein Chem. 47*, 83–229.
32. Tompa, P. (2002) Intrinsically unstructured proteins. *Trends Biochem. Sci. 27*, 527–533.
33. Lacy, E. R., Filippov, I., Lewis, W. S., Otieno, S., Xiao, L., Weiss, S., Hengst, L., and Kriwacki, R. W. (2004) p27 binds cyclin-CDK complexes through a sequential mechanism involving binding-induced protein folding. *Nat. Struct. Mol. Biol. 11*, 358–364.
34. Blundell, T., Lindley, P., Miller, L., Moss, D., Slingsby, C., Tickle, I., Turnell, B., and Wistow, G. (1981) The molecular structure and stability of the eye lens: X-ray analysis of γ-crystallin II. *Nature 289*, 771–777.
35. Mills, I. A., Flaugh, S. L., Kosinski-Collins, M. S., and King, J. A. (2007) Folding and stability of the isolated Greek key domains of the long-lived human lens proteins γD-crystallin and γS-crystallin. *Protein Sci. 16*, 2427–2444.
36. Hemmingsen, J. M., Gernert, K. M., Richardson, J. S., and Richardson, D. C. (1994) The tyrosine corner: A feature of most Greek key β-barrel proteins. *Protein Sci. 3*, 1927–1937.
37. Teintze, M., Inouye, M., and Inouye, S. (1988) Characterization of calcium-binding sites in development-specific protein S of *Myxococcus xanthus* using site-specific mutagenesis. *J. Biol. Chem. 263*, 1199–1203.
38. Villamil Giraldo, A. M., Lopez, M. M., Gonzalez, L. M., Pagano, R. S., Labriola, C. A., Landolfo, L., Delfino, J. M., Parodi, A. J., and Caramelo, J. J. (2010) The structure of calreticulin C-terminal domain is modulated by physiological variations of calcium concentration. *J. Biol. Chem. 285*, 4544–4553.
39. Del, C. N., Jeffery, E., Rizvi, S. M., Stamper, E., Peters, L. R., Brown, W. C., Provoda, C., and Raghavan, M. (2010) Modes of calreticulin recruitment to the major histocompatibility complex class I assembly pathway. *J. Biol. Chem. 285*, 4520–4535.
40. Dowd, T. L., Rosen, J. F., Mints, L., and Gundberg, C. M. (2001) The effect of Pb^{2+} on the structure and hydroxyapatite binding properties of osteocalcin. *Biochim. Biophys. Acta 1535*, 153–163.